

Simultaneous independent measurements of a truncated inner accretion disc in the low/hard state of GX 399–4

D. S. Plant^{1,2}, K. O’Brien¹ and R. P. Fender¹

¹*Department of Physics, Astrophysics, University of Oxford, Keble Road, Oxford, OX1 3RH, UK*

²*School of Physics and Astronomy, University of Southampton, Highfield, Southampton, SO17 1BJ, UK*

28 January 2021

ABSTRACT

We present results from three recent *XMM-Newton* observations of GX 399–4 in the low/hard state, taken during the decay of a bright (peak $\sim 0.05 L_{\text{Edd}}$) failed outburst. Uniquely, these are the first *XMM-Newton* EPIC-pn observations of this source using an imaging mode, which significantly enhances the quality of the data at hand. In particular, thanks to the larger available bandpass, this allows an unprecedented constraint of the thermal accretion disc component, and the level of photoelectric absorption. We simultaneously measured the inner radius of the accretion disc via the broadened Fe $K\alpha$ line and the disc component. The two methods agree, and the measured radii show good consistency over the three epochs. We find that the inner radius is at 20–30 r_g , adding to the growing direct evidence for truncation of the inner accretion disc in the low/hard state.

Key words: accretion, accretion discs - black hole physics - relativistic processes - X-rays: binaries

1 INTRODUCTION

One of the most debated topics in the black hole X-ray binary (BHXR) community is the accretion geometry in the canonical low/hard (hereafter ‘hard’) state. The majority of BHXBs exhibit bright (up to $L_X \sim L_{\text{Edd}}$) outbursts, which are separated by long periods of quiescence. During an outburst, a source transitions between the hard state, dominated by a hard power-law component peaking at ~ 100 keV, and the soft state, where the spectrum peaks around ~ 1 keV, and instead displays a quasi-blackbody shape. Outbursts *always* begin and end in the hard state (see Remillard & McClintock 2006; Fender & Belloni 2012 for recent reviews of BHXB states). Some models predict that in quiescence ($\lesssim 10^{-6} L_{\text{Edd}}$) the accretion disc is substantially truncated ($> 100 r_g$; Narayan et al. 1996; Esin et al. 1997), and in the soft state there is strong evidence that the accretion disc is at the innermost stable circular orbit (ISCO; Gierliński & Done 2004; Steiner et al. 2010; Dunn et al. 2011). It is likely, therefore, that the hard state represents a period of transition in the accretion geometry, but when, and how, this occurs, is of much debate.

The truncated disc model is based around the radiatively inefficient flow solutions (e.g. ADAFs; see Yuan & Narayan 2014 for a recent review), which are able to successfully explain accretion at very low \dot{M} . In this regime, the truncated disc gradually penetrates further into the hot flow as the accretion rate rises (Remillard & McClintock 2006; Done et al. 2007). This is able to explain a number of observables at increasing accretion rates; such as the softening of the power-law component, low reflection fractions, and the increase of characteristic frequencies in the power spectra (van der Klis 2006; Done et al. 2007; Plant et al. 2014a).

However, direct measurements of the inner disc radius have provided conflicting evidence as to whether the disc is truncated or not in the hard state.

The two leading spectroscopic methods to measure the disc inner radius come via the thermal accretion disc component and the broadened Fe $K\alpha$ line (see McClintock et al. 2011 and Reynolds 2013 for the details of these two techniques). Attempts to determine the inner radius of the disc in this manner have led to conflicting results; some evidence suggests that the accretion disc may be at the ISCO as low as $10^{-3} L_{\text{Edd}}$ (Rykoff et al. 2007; Tomsick et al. 2008; Reis et al. 2010), whereas other works, sometimes re-analysing the same data, suggest the accretion disc may be truncated throughout the hard state (e.g. Gierliński et al. 2008; Done & Diaz Trigo 2010; Plant et al. 2014b; Kolehmainen et al. 2014). Key to resolving this debate is simultaneous measurements of the inner disc radius using the two methods. However, a recent study by Kolehmainen et al. (2014), using *XMM-Newton* EPIC-pn timing mode observations of four BHXBs, found the disc and reflection derived inner radii to be inconsistent.

In this letter, we simultaneously measure the disc and reflection inner radius using three recent *XMM-Newton* observations of the black hole GX 399–4 taken in the EPIC-pn small window science mode. These data can potentially achieve a much better constraint on the accretion disc component due to the unprecedented bandpass calibration down to ~ 0.4 keV, thus offering the most stringent test yet of the truncated disc model. In §2 we introduce the observations and the data reduction procedure, and then present our analysis in §3. We find that both methods agree that the accre-

ObsID	Date (UTC)	Exposure (s)	Count Rate (counts s ⁻¹)
1	0692341201	2013-09-29 23:10:18	8 540
2	0692341301	2013-09-30 22:50:37	9 426
3	0692341401	2013-10-01 18:46:27	15 036

Table 1. Observation log of the *XMM-Newton* datasets taken in September–October 2013, which we analyse in this study. Net exposures correspond to that remaining after the reduction process and the live time of the science mode (71 per cent) is taken into account. Count rates in brackets refer to the count rate after the data have been corrected for pile-up.

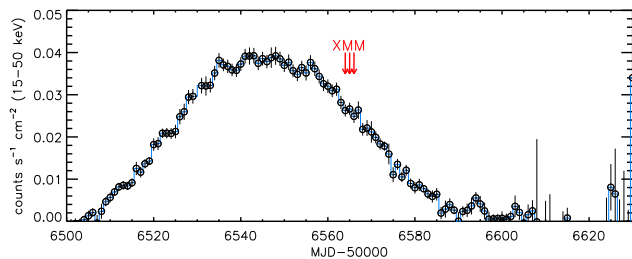


Figure 1. A Swift-BAT (15–50 keV) light-curve of the 2013 failed outburst of GX 339–4. The three *XMM-Newton* observations used in this study are indicated, which caught the source after the peak of the outburst. The source remained in the hard state for the duration of the outburst.

tion disc is truncated, and the impact of this result is discussed in §4.

2 OBSERVATIONS AND DATA REDUCTION

GX 339–4 was observed three times with *XMM-Newton* over a period of three days (Table 1). These observations took place during the decay of a failed outburst, which reached a peak X-ray luminosity of $\sim 0.05 L_{\text{Edd}}$ (Fig. 1). The EPIC-pn and EPIC-MOS cameras were operated in their small window modes, and the ‘thin’ optical blocking filter was used. For this analysis we only used the EPIC-pn data, since the EPIC-MOS suffers significantly more from the effects of pile-up (by a factor of > 5 ; XMM Users Handbook).

Using the *XMM-Newton* Science Analysis System (SAS) version 13.5.0, the raw observation data files (ODFs) were reduced using the tool EPPROC, and the most recent current calibration files (CCFs) were applied. Spectra were extracted through EVSELECT, using a circular region centred on the source with a radius of 45 arcsec. Only single and double events (PATTERN ≤ 4) were used, and bad pixels were ignored (#XMMEA_EP and FLAG==0). Background regions were extracted using a circular region of the same size located away from the source. Using the standard tools, response and ancillary files were created (RMFGEN and ARFGEN), and the spectra were required to have at least 20 counts per channel using the FTOOL GRPPHA. The nominal calibrated bandpass of the EPIC-pn small window mode is 0.3–10 keV; however, we found there to be a strong residual in the pattern distributions created by EPATPLOT below 0.4 keV for all three observations. This was observed as a dip/peak in the single/double distributions, and has been observed a number of times in small window mode datasets. We expect the origin of these features to be from background noise, and they were greatly reduced, but still present, when a background event file was included (withbackgroundset=yes in EPAT-

Parameter	Model–1	Model–2	Model–2b
Observation 1			
N_{H} (10^{22} cm ⁻²)	0.50 ± 0.01	0.64 ± 0.02	0.64 ± 0.02
A_{O}			1.34 ± 0.06
T_{in} (keV)		0.20 ± 0.01	0.19 ± 0.01
N_{DBB} (10^3)		$10.76^{+4.86}_{-3.53}$	$24.83^{+9.40}_{-7.21}$
Γ	1.62 ± 0.01	1.62 ± 0.01	1.63 ± 0.01
N_{Comp}	0.16 ± 0.01	0.16 ± 0.01	0.17 ± 0.01
χ^2/ν	2233/1705	2026/1703	1943/1702
Observation 2			
N_{H} (10^{22} cm ⁻²)	0.50 ± 0.01	0.61 ± 0.02	$0.61^{+0.02}_{-0.01}$
A_{O}			1.30 ± 0.06
T_{in} (keV)		0.22 ± 0.02	0.20 ± 0.01
N_{DBB} (10^3)		$5.77^{+2.67}_{-1.92}$	$13.32^{+5.37}_{-4.02}$
Γ	1.62 ± 0.01	1.60 ± 0.01	1.61 ± 0.01
N_{Comp}	0.16 ± 0.01	0.16 ± 0.01	0.16 ± 0.01
χ^2/ν	2379/1743	2173/1741	2106/1740
Observation 3			
N_{H} (10^{22} cm ⁻²)	0.49 ± 0.01	0.61 ± 0.02	0.61 ± 0.02
A_{O}			1.34 ± 0.05
T_{in} (keV)		0.22 ± 0.01	0.20 ± 0.01
N_{DBB} (10^3)		$5.56^{+1.91}_{-1.48}$	$13.05^{+3.14}_{-3.97}$
Γ	1.61 ± 0.01	1.59 ± 0.01	1.60 ± 0.01
N_{Comp}	0.15 ± 0.01	0.15 ± 0.01	0.15 ± 0.01
χ^2/ν	2610/1790	2220/1788	2092/1787

Table 2. Results from various continuum model fits.

Model–1: TBNEW_FEO*(NTHCOMP)

Model–2: TBNEW_FEO*(DISKBB+NTHCOMP)

Model–2b: The same as Model–2, but the O abundance in TBNEW_FEO (A_{O}) is now a free parameter.

PLOT). The features were strongest in Observation 3, which occurred at the start of orbit 2530, thus it is likely that they are due to background radiation. We therefore applied a lower limit of 0.4 keV for all of the spectra, and we also ignored the 1.75–2.35 keV region where strong features were observed. These are often seen when observing bright sources, and are likely to be of instrumental origin.

We applied the SAS tool EPATPLOT to all of the datasets to check for photon and pattern pile-up, which was found to be high in all three observations. To mitigate the pile-up we investigated a number of annulus extraction regions for the spectra, and found an inner cavity with a radius of 11.5 arcsec to be very acceptable. This reduced the estimated level of pile-up to be less than 1 per cent for both the single and double events between 0.4–10 keV. All of the analysis in this letter was performed using XSPEC v.12.8.0, and all quoted errors are at the 90 per cent confidence level. We use the ‘wilm’ abundances and ‘vern’ cross-sections for all of the analysis.

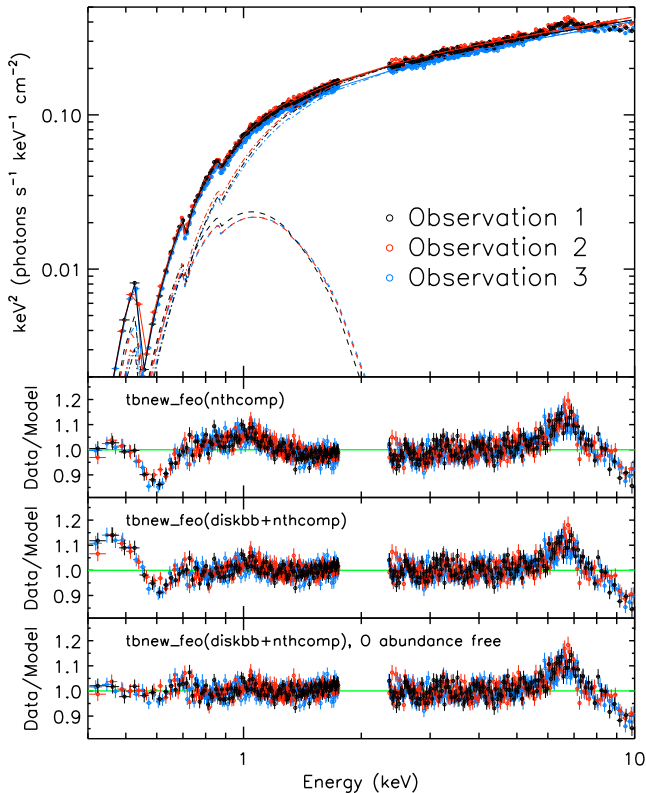


Figure 2. Unfolded spectra and model residuals to the best-fit continuum model (Model–2b; Table 2). There is a clear excess and edge around 7 keV, which strongly suggests an Fe emission line corresponding edge is present in the spectra. Solid, dash and dot-dash lines describe the total, DISKBB and NTHCOMP model components respectively.

3 ANALYSIS AND RESULTS

The hard state X-ray spectrum of BHRBs is often successfully modelled with a power-law, which is most commonly associated with inverse Comptonisation of photons in a corona of hot (~ 100 keV) electrons. Therefore, to begin, we fit each spectrum with an absorbed power-law (TBNEW_FEO*POWERLAW in XSPEC; Wilms et al. 2000). The fit was reasonable ($\chi^2_\nu = 1.43/5238$; Table 2), and both the photon index and column density were typical for GX 339–4 in the hard state (e.g. Kolehmainen et al. 2014).

However, a power-law is not a physical model, and can lead to an excess of photons at low energies. Assuming that the hard power-law tail arises through Comptonisation of disc photons, there should be a low-energy cut-off associated with the disc temperature. Thermal Comptonisation is the favoured interpretation for the hard state power-law (see Done et al. 2007 for a detailed review), thus we replaced the POWERLAW model with NTHCOMP (Zdziarski et al. 1996). This model includes a high energy cutoff, parameterised by the electron temperature kT_e , which we fixed to be 50 keV (Done et al. 2007). Because of the soft bandpass used in this study, this parameter could not be constrained, but the cut-off is not expected to be low enough to affect the spectrum < 10 keV. This model also includes a low energy rollover, defined by a seed photon temperature kT_{bb} , which we fixed to be 0.2 keV (a typical value for the hard state; Reis et al. 2010; Kolehmainen et al. 2014). To this end, we also set the seed spectrum to be a disc-blackbody. The other free parameters were the photon index and normalisation,

Parameter	Observation 1	Observation 2	Observation 3
N_H (10^{22} cm $^{-2}$)	$0.76^{+0.01}_{-0.02}$	0.74 ± 0.01	$0.74^{+0.03}_{-0.02}$
A_O	$1.52^{+0.03}_{-0.06}$	$1.50^{+0.05}_{-0.04}$	$1.55^{+0.04}_{-0.02}$
T_{in} (keV)	0.16 ± 0.01	0.16 ± 0.01	0.17 ± 0.01
N_{DBB} (10^5)	$1.34^{+0.28}_{-0.18}$	$1.09^{+0.21}_{-0.19}$	$0.89^{+0.43}_{-0.20}$
$r_{in}(DBB)$ (r_g)	25^{+3}_{-2}	29 ± 3	26^{+3}_{-6}
Γ	1.62 ± 0.02	1.65 ± 0.01	$1.59^{+0.02}_{-0.03}$
N_{Comp}	0.092 ± 0.01	0.14 ± 0.01	0.08 ± 0.01
$r_{in}(Fe)$ (r_g)	21^{+17}_{-9}	27^{+6}_{-6}	16^{+7}_{-4}
i ($^\circ$)		30^{+5}_{-4}	
$\log \xi$ (erg cm s $^{-1}$)	3.17 ± 0.06	$3.03^{+0.05}_{-0.03}$	$3.17^{+0.06}_{-0.05}$
N_{Fe} (10^{-6})	0.34 ± 0.03	$0.26^{+0.03}_{-0.04}$	$0.32^{+0.03}_{-0.02}$
χ^2/ν	5322/5219		

Table 3. The best-fit model and MCMC derived 90 per cent confidence limits for fits to the three GX 339–4 observations. The inclination parameter is fitted jointly between the three spectra. ‘DBB’ and ‘Fe’ refer to the DISKBB and RELXILL components respectively.

tion, like for the POWERLAW model. Using NTHCOMP the fit was slightly improved ($\chi^2_\nu/\nu = 1.38/5238$; Table 2), but not significantly.

A strong excess at ~ 7 keV, and drop above 8.5 keV, were clear (Fig. 2), suggesting that a significant amount of reflection was present, which is ubiquitously observed in the hard state of GX 339–4 (see e.g. Dunn et al. 2008; Plant et al. 2014a). Also, an excess peaking at ~ 1 keV, and a strong edge at 0.6 keV, were further clear residuals in the spectra. The excess at ~ 1 keV is likely to be due to thermal emission from the accretion disc, which is often observed from hard state sources with soft X-ray instruments (Miller et al. 2006; Reis et al. 2010; Kolehmainen et al. 2014). We therefore added a multi-colour disc-blackbody model (DISKBB; Mitsuda et al. 1984), which considerably improved the fit ($\chi^2_\nu/\nu = 1.22/5232$; Table 2). The disc component contributes ~ 17 per cent of the total unabsorbed 0.4–10 keV flux.

However, the fit was still poor < 0.7 keV (Fig. 2), the main cause of which was a strong edge-like feature at ~ 0.6 keV, coincident with the O K edge at 0.54 keV (see e.g. Wilms et al. 2000). We therefore allowed the O abundance to be a free parameter, which further improved the fit ($\chi^2_\nu/\nu = 1.17/5229$; Table 2). All of the observations settled on an O abundance of ~ 1.34 , and meant that the soft bandpass was now excellently fit ($\chi^2_\nu = 1.04$ below 5 keV).

As can be seen in Fig. 2, a strong Fe K α emission line and corresponding edge were still present in the spectra. To model this we added the X-ray reflection model RELXILL (García et al. 2014), which combines the relativistic RELCONV code of Dauser et al. (2010) with the angle-resolved X-ray reflection table XILLVER of García et al. (2013). This represents the first code to prescribe the correct reflection spectrum for each relativistically calculated emission angle, as opposed to the usual relativistic convolution treatment to the spectrum (e.g. RELCONV*XILLVER).

We fixed the spin to be 0.9^1 , and assumed an emissivity profile

¹ A spin of 0.9 is a compromise between previous conflicting spin measurements of GX 339–4 (Reis et al. 2008; Kolehmainen & Done 2010). We tested different values (0, 0.5, 0.998) and found them to not affect the results, which should be expected since the spin has little effect on the Fe profile for the values of r_{in} we measure (Dauser et al. 2010).

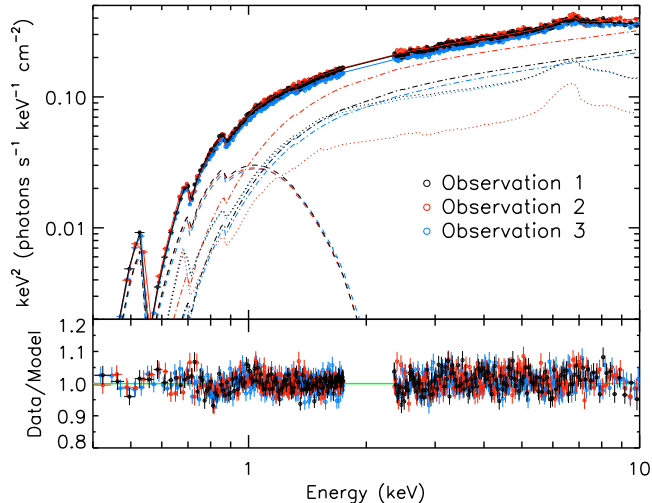


Figure 3. Unfolded spectra and model residuals to the best-fit continuum+reflection model (Table 3), which represents an excellent fit over the entire bandpass. Solid, dash, dot-dash and dotted lines describe the total, DISKBB, NTHCOMP and RELXILL model components respectively.

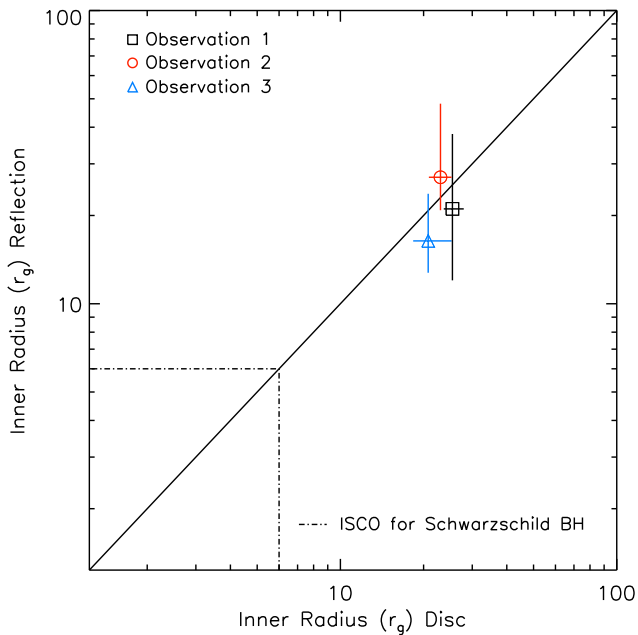


Figure 4. The inner radius of the accretion disc, fitted by the disc (x-axis) and reflection (y-axis) components (Table 3). The dot-dash line indicates the innermost stable circular orbit for a zero spin black hole, showing that both methods, from all three observations, are consistent with a truncated accretion disc.

of R^{-3} . We also linked the photon index in NTHCOMP to the illuminating index in RELXILL. The ionisation parameter ξ , the disc inner radius r_{in} , and the model normalisation were all fitted freely. Finally, the inclination was fitted jointly by the three spectra. For all three observations the inner radius was found to be moderately truncated at $\sim 20 r_g$, and the fit was excellent over the whole bandpass ($\chi^2_{\nu} = 1.02/5219$; Fig. 3). Given the excellent constraint on the disc emission allowed by the 0.4–10 keV bandpass, we were able to compare how the inner radius derived from the disc component

compares to that from the reflection. The normalisation of DISKBB is defined as

$$N_{\text{BB}} = 1.19 \left(\frac{r_{\text{in}}}{D_{10 \text{ kpc}}} \right)^2 \cos i \quad (1)$$

where D is the distance to the source in units of 10 kpc, r_{in} is the disc inner radius in km, and i is the inclination of the disc, which we assumed to be the same as fitted by the reflection component (Table 3). The 1.19 factor accounts for the spectral hardening factor f_{col} and that T_{in} occurs at a radius somewhat larger than r_{in} (Kubota et al. 1998). We find that the inner radii derived from the disc and reflection are very consistent. To probe this connection further we performed a Markov Chain Monte Carlo (MCMC) analysis on the best-fit parameters. Six 55,000 element chains were produced, of which the first 5000 elements were discarded (‘burnt’). Each chain was run from a random perturbation away from the best fit, and the chain proposal was taken from the diagonal of the subsequent covariance matrix. The probability distributions were assumed to be Gaussian, and a rescaling factor of 5×10^{-4} was applied. The confidence limits derived from the resultant 300,000 element chain are presented in Table 3.

The agreement between the inner radii calculated from the reflection and disc components is very good, despite the relatively short exposure of the data. Figure 4 compares the respective radii and presents compelling evidence that the inner disc is truncated at $20\text{--}30 r_g$. Furthermore, the disc component radii are extremely consistent between the three observations, despite the weakness of the component in the hard state. The confidence limits of the reflection radii are larger, but still good considering the relatively short exposures and low flux of the system.

Recent works have shown that the emissivity profile is complex close to the black hole ($< 10 r_g$; Wilkins & Fabian 2012; Dauser et al. 2013). We therefore relaxed the assumption that the emissivity profile is R^{-3} ; however, rather than fitting a broken power-law emissivity, which is not at all physical, we instead switched to an additional version of RELXILL called RELXILLP. This model fits the height of the illuminating X-ray source, applying the corresponding emissivity profile to the reflection spectrum (Dauser et al. 2013; García et al. 2014). This model can also self-consistently fit the power-law and reflection components, ensuring that the correct reflection fraction is computed as a function of source height and disc inner radius. We therefore removed NTHCOMP and allowed RELXILLP to self-consistently fit the two components. We find that the results are very consistent with those assuming R^{-3} , and the fit is improved ($\Delta\chi^2 = -21$; Table 4). In particular, the disc inner radius fitted from both the disc and reflection components is almost unchanged. The fitted source height h is consistent within errors over the three observations, and is measured to be at $14\text{--}70 r_g$ (90 per cent confidence). The constraint on h is poor since the emissivity profiles of a broad range of source heights converge at the values of r_{in} being fitted (Dauser et al. 2013). Much better constraints on h should be possible at higher accretion rates when the disc is expected to be less truncated.

4 DISCUSSION AND CONCLUSIONS

In this letter, we have presented analysis of three recent observations of GX 339–4 in the hard state during the decay phase of a failed outburst. These observations utilised the small window science mode, and represent one of the first hard state observations of a black hole using an *XMM-Newton* EPIC-pn imaging mode.

Parameter	Observation 1	Observation 2	Observation 3
$h(r_g)$	37^{+33}_{-13}	17^{+5}_{-3}	26^{+18}_{-7}
$r_{\text{in (DBB)}}(r_g)$	25 ± 2	29 ± 3	26^{+3}_{-1}
$r_{\text{in (Fe)}}(r_g)$	20^{+4}_{-5}	29 ± 2	16 ± 2
$i(^{\circ})$		33 ± 3	
χ^2/ν		5301/5219	

Table 4. The best-fit model and MCMC derived 90 per cent confidence limits for the fit with RELXILLP. All of the parameters not listed in this table were consistent within errors with those in Table 3. The inclination parameter was again fitted jointly between the three spectra.

This presents a well calibrated bandpass down to 0.4 keV, whereas the fast modes that are usually employed are restricted to above 0.7 keV. The result is an unprecedented view of the accretion disc component, which typically peaks at ~ 0.2 keV in the hard state. This also removes the calibration uncertainties associated with the fast modes; such as reliable pile-up correction (see Miller et al. 2010), the lack of source-free background regions (Ng et al. 2010), and issues with charge-transfer inefficiency at high count rates (Walton et al. 2012).

Aided by the excellent constraint of the disc component we were able to measure the inner radius from both the disc and reflection components, which both agree on a moderately truncated inner disc. The jointly fit inclination is, however, smaller than expected, given the mass function constraint of Muñoz-Darias et al. (2008). As shown in Plant et al. (2014b), a higher fitted inclination would act to increase the reflection inner radius, since the larger doppler shifts at higher inclination broaden the Fe profile. We performed fits with larger fixed values of i , which confirmed that the fitted reflection inner radius does indeed increase. The fitted radii are considerably smaller than those found in the hard state of GX 339–4 by Plant et al. (2014b) and Kolehmainen et al. (2014); however, this is, at least in part, due to the smaller inclination. From Eq. 1, it is clear that larger i would have the same effect on the inner radius measured by the disc component.

To conclude, this is the first time that the disc and reflection methods have been able to simultaneously test truncation of the inner accretion disc in the hard state. This adds to recent direct evidence for truncation in the hard state, which together are finally establishing certainty in the hard state accretion geometry.

ACKNOWLEDGEMENTS

DSP acknowledges financial support from the STFC. This project was funded in part by European Research Council Advanced Grant 267697 4-pi-sky: Extreme Astrophysics with Revolutionary Radio Telescopes. This letter is based on observations obtained with *XMM-Newton*, an ESA science mission with instruments and contributions directly funded by ESA Member States and the USA (NASA).

REFERENCES

Dauser T., Garcia J., Wilms J., Böck M., Brenneman L. W., Falanga M., Fukumura K., Reynolds C. S., 2013, *MNRAS*, 430, 1694

Dauser T., Wilms J., Reynolds C. S., Brenneman L. W., 2010, *MNRAS*, 409, 1534

Done C., Diaz Trigo M., 2010, *MNRAS*, 407, 2287

Done C., Gierliński M., Kubota A., 2007, *A&AR*, 15, 1

Dunn R. J. H., Fender R. P., Körding E. G., Belloni T., Merloni A., 2011, *MNRAS*, 411, 337

Dunn R. J. H., Fender R. P., Körding E. G., Cabanac C., Belloni T., 2008, *MNRAS*, 387, 545

Esin A. A., McClintock J. E., Narayan R., 1997, *ApJ*, 489, 865

Fender R., Belloni T., 2012, *Science*, 337, 540

García J. et al., 2014, *ApJ*, 782, 76

García J., Dauser T., Reynolds C. S., Kallman T. R., McClintock J. E., Wilms J., Eikmann W., 2013, *ApJ*, 768, 146

Gierliński M., Done C., 2004, *MNRAS*, 347, 885

Gierliński M., Done C., Page K., 2008, *MNRAS*, 388, 753

Kolehmainen M., Done C., 2010, *MNRAS*, 406, 2206

Kolehmainen M., Done C., Díaz Trigo M., 2014, *MNRAS*, 437, 316

Kubota A., Tanaka Y., Makishima K., Ueda Y., Dotani T., Inoue H., Yamaoka K., 1998, *PASJ*, 50, 667

McClintock J. E. et al., 2011, *Classical and Quantum Gravity*, 28, 114009

Miller J. M. et al., 2010, *ApJ*, 724, 1441

Miller J. M., Homan J., Miniutti G., 2006, *ApJL*, 652, L113

Mitsuda K. et al., 1984, *PASJ*, 36, 741

Muñoz-Darias T., Casares J., Martínez-Pais I. G., 2008, *MNRAS*, 385, 2205

Narayan R., McClintock J. E., Yi I., 1996, *ApJ*, 457, 821

Ng C., Díaz Trigo M., Cadolle Bel M., Migliari S., 2010, *A&A*, 522, A96

Plant D. S., Fender R. P., Ponti G., Muñoz-Darias T., Coriat M., 2014a, *MNRAS*, 442, 1767

Plant D. S., Fender R. P., Ponti G., Muñoz-Darias T., Coriat M., 2014b, *A&A*, in press (arXiv:1309.4781)

Reis R. C., Fabian A. C., Miller J. M., 2010, *MNRAS*, 402, 836

Reis R. C., Fabian A. C., Ross R. R., Miniutti G., Miller J. M., Reynolds C., 2008, *MNRAS*, 387, 1489

Remillard R. A., McClintock J. E., 2006, *ARAA*, 44, 49

Reynolds C. S., 2013, *Space Sci. Rev.*

Rykoff E. S., Miller J. M., Steeghs D., Torres M. A. P., 2007, *ApJ*, 666, 1129

Steiner J. F., McClintock J. E., Remillard R. A., Gou L., Yamada S., Narayan R., 2010, *ApJL*, 718, L117

Tomsick J. A. et al., 2008, *ApJ*, 680, 593

van der Klis M., 2006, *Rapid X-ray Variability*, Lewin W. H. G., van der Klis M., eds., Cambridge Univ. Press, Cambridge, pp. 39–112

Walton D. J., Reis R. C., Cackett E. M., Fabian A. C., Miller J. M., 2012, *MNRAS*, 422, 2510

Wilkins D. R., Fabian A. C., 2012, *MNRAS*, 424, 1284

Wilms J., Allen A., McCray R., 2000, *ApJ*, 542, 914

Yuan F., Narayan R., 2014, *ArXiv e-prints*

Zdziarski A. A., Johnson W. N., Magdziarz P., 1996, *MNRAS*, 283, 193